IEEE Access
Multidisciplinary | Rapid Review | Open Access Journal

Received 14 June 2022, accepted 29 June 2022, date of publication 5 July 2022, date of current version 12 July 2022.

Digital Object Identifier 10.1109/ACCESS.2022.3188686

RESEARCH ARTICLE

Control Hardware in the Loop and IoT Integration: A Testbed for Residential Photovoltaic System Evaluation

VÍCTOR SÁMANO-ORTEGA[1], HUGO MÉNDEZ-GUZMÁN[1], JOSÉ PADILLA-MEDINA[2], JUAN AGUILERA-ÁLVAREZ[1], CORAL MARTÍNEZ-NOLASCO[1], AND JUAN MARTÍNEZ-NOLASCO[3]

[1]Doctorado en Ciencias de la Ingeniería, Tecnológico Nacional de México/IT de Celaya, Celaya 38010, Mexico
[2]Departamento de Ingeniería Electrónica, Tecnológico Nacional de México/IT de Celaya, Celaya 38010, Mexico
[3]Departamento de Ingeniería Mecatrónica, Tecnológico Nacional de México/IT de Celaya, Celaya 38010, Mexico

Corresponding author: Juan Martínez-Nolasco (juan.martinez@itcelaya.edu.mx)

ABSTRACT This article presents the development of a platform for the validation of controllers applied to photovoltaic systems (PVS) interconnected with the main grid (MG), integrating simulation real-time Hardware in the Loop (HIL) and Internet of Things (IoT). The proposed platform is made up of 5 parts: 1) a control HIL emulator (CHILE) that reproduces the behavior of a photovoltaic array, a power electronic converter for interconnection with the MG, and AC loads, 2) a cloud database implemented in ThingSpeak, 3) a smart sensor (SS) that monitors the behavior of AC loads, 4) a residential PVS with internet connection, and 5) an Android application for remote monitoring. The data generated by the residential system and the SS are stored in the database and from this information the CHILE reproduces its behavior in real time. The CHILE generates the variables related to the behavior of the PVS and transfers this information to the database. The mobile application allows users to view the behavior of the platform remotely. The usefulness of the platform is verified with a controller for the maximum power point tracking and the interconnection of the system with the MG in a 24-hour experiment, during which the behavior of the residential PVS and the AC loads are reproduced in the CHILE. The platform successfully emulates the behavior of the installed PVS with a mean relative error of 0.42% and the AC load with a mean absolute error of 10 mA. Regarding data transfer in the IoT network, a mean time response of the server of 441.9 ms was observed without data loss during the 24-hours experiment.

INDEX TERMS Control hardware in the loop, IoT, photovoltaic system.

I. INTRODUCTION

Among the different existing renewable energy sources, photovoltaics is considered a clean and safe technology for electricity generation [1]. This technology does not have moving parts, it can be located on rooftops, its maintenance cost is low, and with an interconnected system to the main grid (MG) the electricity bill and dependence on the MG are reduced, therefore the grid-connected photovoltaic systems (PVS) are the most popular renewable energy generation technology in the residential sector [2]. The power electronics converters (PEC), which convert the DC energy generated by the photovoltaic arrays (PA) into AC energy compatible with the MG, are key elements in the grid-connected residential photovoltaic system (GcRPVS) because they allow the energy transfer to the MG. Therefore, these systems require sophisticated control structures to manage the energy flow to the MG and obtain better system performance [3]. However, the energy generated by a GcRPVS is highly dependent on atmospheric variables, this implies its design and control must be evaluated and validated to guarantee its optimal operation [4].

The associate editor coordinating the review of this manuscript and approving it for publication was Taehong Kim.

One option for experimentation is real-time Hardware in the Loop (HIL) simulation. This technique consists of placing a physical element in a controllable environment to validate its operation; in this environment the interactions of the system under test with adjacent elements are emulated in hardware [5]. If the element under test comprises the controller of a physical system, or part of it, while the rest of the system is emulated in hardware, the HIL simulation is classified as control HIL (CHIL) [6]. With a CHIL simulation it is possible to validate real controllers under operating conditions like those that will be submitted in its final application [7]. The CHIL technique has been used to validate PVS controllers in works such as [8]–[10].

Lately, Internet of Things (IoT) together with storage and/or computing in cloud are used widely for developing monitoring systems in multiple fields. In [11] a smart healthcare video surveillance system is proposed. In this research, the time response and network bandwidth are reduced integrating background subtraction and deep convolution neural network algorithms on moving objects in the FOG layer. In [12], an IoT and deep learning integration for online fault diagnosis of power transformers is proposed. In this research, a one-dimension convolutional neural network for the fault diagnosis and cyberattack detection was developed. The neural network determines the kind of fault based on gas concentration in the insolating oil with an accuracy of 94.36% under normal conditions and 92.58% considering cyberattacks. Finally, in [13] an IoT and deep learning neural network integration for online CNC machines monitoring is presented. The proposed platform classifies the machine operation into stable, unstable, and attacked, the latter in the case of an cyberattack, depending on the workpiece forces exerted by the machine. In this research the MQTT protocol is used for the communication network.

On the other hand, the new concepts such as IoT and ''Energy Internet'' (EI) have been recently introduced in energy systems. These concepts refer to the integration of an energy system and information and communication technologies [14]. Recent research uses EI, employing IoT, in PVS, some examples are described below. In [15] an IoT platform for PVS supervision using open-source technologies is reported, this platform uses a Moxa UC-2112 PC with Kura software along with IoT Gateway and an MQTT broker developed on the Kapua platform, the proposed platform was validated in a 3 MW plant. In [16] a monitoring IoT network for decentralized PVS is described, the network has 3 main parts: monitoring devices developed with ESP32 and ESP8266 modules, a cloud server with a MySQL database and a PHP web monitor for the visualization of the data. The network monitors PA temperature, solar radiation, relative humidity, room temperature, and wind speed in three PVS. In [17] a recurrent neural network is proposed to predict the power generated by a PVS in the short term; IoT sensors that monitor the PVS in real time were used to feed the neural network. Also researches that integrate IoT and HIL in energy systems have been reported: in [18] a centralized energy management system for a micro-grid (μG) is proposed, the μG is emulated using the HIL technique and the centralized controller maintains communication with the μG through the Internet. In [19] the development of a power HIL (PHIL) simulation is described using a geographically distributed infrastructure that is composed of a real-time simulator and a Back-to-Back PEC, separated from each other by approximately 40 km of distance and maintaining communication over the internet. In [20] the development of a geographically distributed PHIL simulation is detailed, the infrastructure of this simulation is composed of two laboratories, one in Bari and the other in Turin, separated by approximately 1000 km. The laboratories communicate with each other through a VPN tunnel that uses cybersecurity and a UDP protocol. In [21] a HIL simulation of a low voltage distribution network including smart buildings is described. The simulation consists of emulating a distribution network connected with multiple smart buildings, for which the data generated in a real smart building with different loads and sensors is used. The information between the building and the simulation is carried out through an IoT bus. In [22] the development of an architecture that integrates IoT and HIL in a PHIL simulation is detailed. The network integrates real devices with simulated devices for the purpose of using the information obtained from the real devices to create simulated devices with the same characteristics. The real devices connect to the simulation through IoT.

This article describes the development of a platform for the validation of PVS controllers integrating IoT and CHIL (iCHIL). This platform is made up of five parts: a CHIL emulator (CHILE), an RPVS, a smart sensor (SS), a cloud database, and a mobile application. The CHILE reproduces the behavior of a PA, a PEC for interconnection with the MG that integrates a boost PEC and a DC-AC PEC, an AC load, and the MG. The emulator has an analog input that controls the PEC and multiple analog outputs that represent the MG voltage, the PA voltage, the current injected to the MG, the load current, and the boost PEC output voltage. Also, the emulator has an embedded controller to manipulate its behavior. The RPVS is made up of an array of six 370 W panels connected in a series and a single-phase inverter with a single maximum power point tracking (MPPT) with a capacity of 2 KW and an internet connection via Wi-Fi. This inverter has a remote monitoring system in which production data is stored and displayed on a website. The SS measures the voltage and current of an AC load and transfers this information to a cloud database. The production information of the RPVS and the information obtained by the SS are downloaded to the CHILE and with it, this emulator reproduces the behavior of the PVS and the AC load in real-time. In this way, the operating conditions of the emulator are determined by the real behavior of the systems used in a house. The database was developed using ThingSpeak, this software stores the RPVS production data, the SS data, and a series of variables generated by the CHILE. Finally, the mobile application allows the monitoring of the information stored in the database.

The integration of IoT and CHIL technologies, as well as the structure proposed in this study, provide the developed iCHIL platform with the following advantages:

1) The CHILE is developed using generic hardware. This is a low-cost alternative compared to commercial HIL platforms.
2) The mathematical models are embedded using a high-level language, this represents a faster and more reproducible implementation compared to the use of hardware description languages.
3) The structure of the CHILE allows reconfiguring embedded systems as well as integrating quickly and easily new systems to the proposed topology.
4) The platform allows the emulation of the behavior of photovoltaic systems and AC loads under realistic scenarios.
5) The platform allows the emulation f AC loads using data collected by a smart sensor.
6) The platform allows the emulation of a photovoltaic system using data collected from the inverter.
7) The CHILE allows the integration of different controllers for validation.
8) The IoT network and the developed application allow the remote monitoring of the platform.

This article is divided into 6 sections. The first corresponds to the introduction. Section II describes the iCHIL platform and its components. The third section details the IoT communication and monitoring network. In section IV the implementation of the CHILE is described and finally, in sections V and VI correspondingly, the results and conclusions are described.

II. DESCRIPTION OF THE iCHIL PLATFORM

In this section, the development of an iCHIL platform to evaluate the performance of controllers applied in GcRPVS is described. The platform is made up of five parts: 1) the monitoring of the energy production of a GcRPVS, 2) the monitoring of the energy consumption of AC loads, 3) a database in the cloud for storage the information of the generation and energy consumption, 4) a mobile application for viewing the data stored in the cloud, and 5) a CHILE that reproduces the behavior of the GcRPVS and connects to a controller under test. Fig. 1 shows the proposed iCHIL platform structure.

The GcRPVS monitoring is carried out by a web driver developed in Python, which accesses a website that hosts information from the GcRPVS inverter, retrieves the information corresponding to the actual power that the PA produces and stores it in the cloud. In the monitoring of the voltage and current in the AC loads, an SS is used which evaluates the instantaneous power, the phase angle, and the power factor, later this information is stored in the database in the cloud. The database stores the information generated by the web driver, the SS and the CHILE every 16 seconds; Additionally, functions were implemented to evaluate and graph variables from the stored information, which is monitored through an Android application. Finally, the CHILE is made up of two development boards, in the first one a PA was embedded, which based on the production data obtained from the inverter portal reproduces the behavior of the GcRPVS PA, a PEC for interconnection with the MG, composed of a DC-DC converter in cascade with a DC-AC converter, and AC loads that emulate the behavior of the monitored loads. In the second board, a controller for the interconnection of the PVS with the MG was embedded. This controller includes an algorithm for MPPT and two PIs in cascade. Additionally, the CHILE includes a user interface developed in LabVIEW that provides on-site monitoring. With the proposed system it is possible to validate the embedded controller in a scenario that reproduces the operating conditions of a GcRPVS and the AC loads. This is achieved with continuous monitoring of real variables and their simulation in a CHILE. This approach makes it easy to integrate the controller into its final application. The system integrates IoT and HIL technologies to provide a structure that allows a controller to be validated reliably and in a short time in a real scenario and with the possibility of monitoring its operation from anywhere.

In the following sections each one of the elements presented in Fig. 1 is described in detail. The order in which these elements are presented correspond to the enumeration assigned in Fig. 1. Thus, components 1 to 4 are detailed in section III and component 5 in section IV.

As with the GcRPVS, the monitoring AC load has a residential scale. This characteristic defines the range of the signals generated in CHILE, the topology and passive elements of the bidirectional electronic power converter and is the reference for the smart sensor design.

III. COMMUNICATION AND MONITORING NETWORK

A. GcRPVS MONITORING

The proposed GcRPVS is in the city of Celaya, Guanajuato, Mexico and consists of 6 SERAPHIM 370 W panels connected in series, and a 2 kW GOODWE NS series single-phase inverter with a single MPPT with internet connection via Wi-Fi. The supplier of the inverter provides an internet portal for the monitoring of the variables (smart energy management system (SEMS)) with which the behavior of the voltage and current of the PA, the DC and AC power, the generated energy, weather variables among other items are evaluated every 5 minutes. The information on the power generated by the PA is obtained through a web driver developed in Python, which accesses the SEMS. The web driver uses web scraping tools to navigate the site, access the service credentials, analyze the HTML code of the web page, extract the power information, and transfer this information to the cloud database, this is carried out every 5 minutes (See Fig. 2).

B. AC LOADS MONITORING

For the monitoring of AC loads, an SS was developed using a microcontroller, an ESP8266 module, a non-invasive current sensor SCT-013-100, and an HCPL-7800 isolation amplifier.

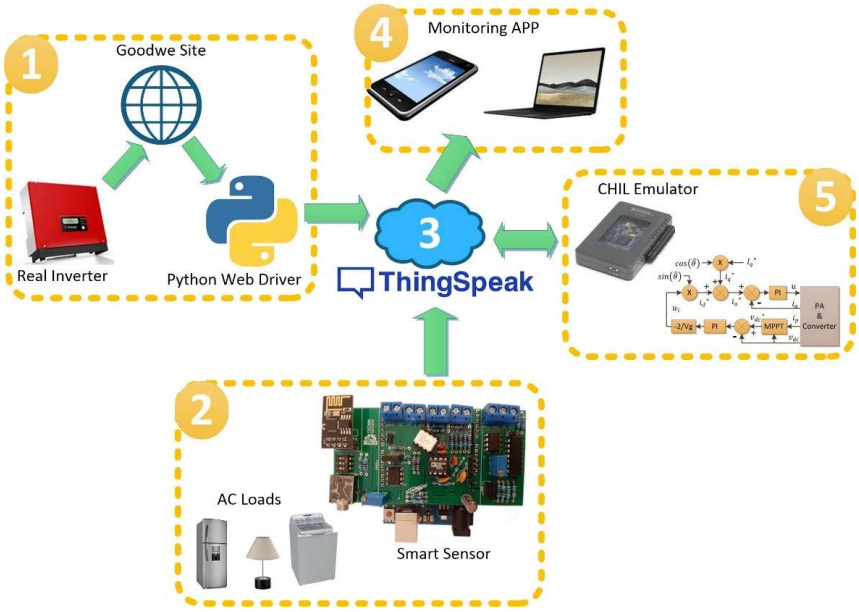

FIGURE 1. iCHIL platform structure.

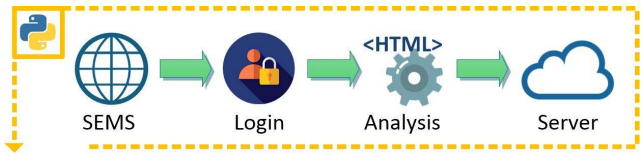

FIGURE 2. Web driver functionality.

The voltage (V_m) and current (I_m) signals are coupled and conditioned to be measured by the microcontroller, which processes the information to calculate the RMS voltage V_g, RMS current I_z, phase angle φ, instantaneous power, and power factor. The microcontroller sends, with HTTP requests, the information to the database through the IoT transmitter (ESP8266 module) with an update rate of 16 seconds. Fig. 3 shows the general scheme of the proposed SS.

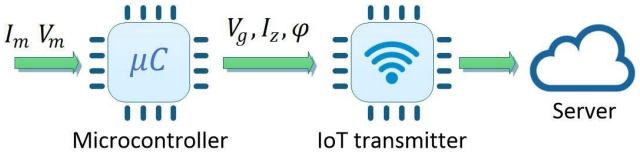

FIGURE 3. SS general scheme.

C. DATABASE

The database used in the iCHIL platform was developed in ThingSpeak, this service integrates a web application, a data base organized in channels with 8 fields each and a REST API for data transferring with the standard HTTP protocol and the methods GET and POST or a MQTT API with the methods Publish and Subscribe. In this research the REST API with the method GET was used for all communication in the network. As Fig. 4 shows, five channels are used, three of which contain the information uploaded by the web driver, the SS and the CHILE (called WD, SS, and HIL in Fig. 4). The remaining two channels are used to store the results of an online analysis that determines variables dependent on the information uploaded in the first three channels. The load RMS voltage, V_g, the RMS current of the load, I_z, and the phase angle, φ, are extracted from the SS channel. With this information, the values of R and L or C are defined to determine if it is a resistive, resistive-capacitive or resistive-inductive load. From the HIL channel, the voltage v_p and the i_p current of the panel are extracted to evaluate the power of the panel in the CHILE $P_p\,|HIL$ and the solar radiation G that produces that power; this action is performed every 5 minutes. Finally, from the WD channel the power generated by the GcRPVS $P_p\,|i$ is extracted and compared with the power of the PA of the CHILE, this comparison is presented to the user graphically through a MATLAB visualization. The data is updated every 16 seconds, considering that the power generated by the GcRPVS and the load consumption change slowly, this rate provides enough information to reproduce the behavior in the CHILE without data loss and avoiding an excessive amount of data stored in it, which could cause a failure because of lack of memory capacity.

D. MOBILE APP

Each element of the iCHIL platform can be viewed through an APP with which the user can access to the information stored on the server. The user defines the variable and the amount of data to display, this information is downloaded from ThingSpeak through HTTP requests and displayed in a Chartview, another option is to choose a visualization to be presented in a Webview. The APP interacts with a local database that stores information in the phone's memory and

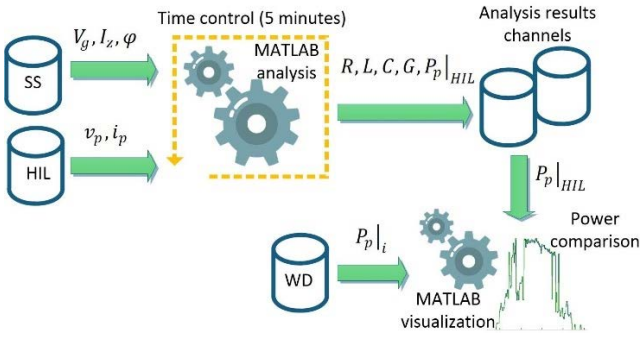

FIGURE 4. Database structure.

allows the user to keep and manage access credentials and channel identifiers, as well as Thingspeak views. Fig. 5 shows a diagram of the functionality of the developed application.

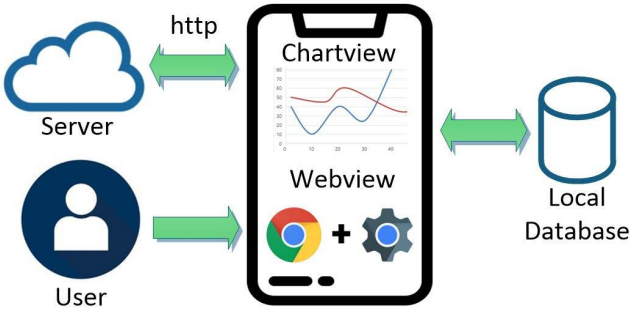

FIGURE 5. Functionality of the APP.

IV. CONTROL HARDWARE IN THE LOOP EMULATOR

In the implementation of the CHILE, two NI myRIO-1900 (myRIO) development boards were used, these boards integrate a real-time processor (RTP) and an FPGA, which are widely employed in the implementation of low-cost HIL platforms [23], in addition to having a clock of 40 MHz [24]. The CHILE is made up of two subsystems: a PVS Emulator (PVSE) and a controller under test (CUT). These elements are each embedded in a myRIO and are intercommunicated. In the case of the PVSE, it has communication with a PC, through the RTP, in which the data stored in the cloud is downloaded to determine the state of the GcRPVS and the load. This information is used to define the operating state of the emulator. The FPGA of this emulator reproduces the behavior of the PA, the PEC, the load, and the MG. As for the CUT, it is divided into two parts: a controller for the MPPT was embedded in the RTP and in the FPGA a PLL, the calculation of the reference reactive current i_q^* (RR), and a main control structure composed of two PI in cascade were embedded. Fig. 6 shows the CHILE scheme.

The discretized mathematical model of the elements represented in Fig. 6 are solved by hardware in the FPGA of each one of the myRIO. With these, digital signals are generated and then are converted into analog signals and vice versa. In the case of RTP, the implementations are of the software type, so from there, the signals are handled as data. Communication between the FPGA and the RTP is done through the ARM Advanced Microcontroller Bus Architecture (AMBA) standard.

A. PHOTOVOLTAIC SYSTEM EMULATOR

The topology to emulate the GcRPVS consists of the serial connection of a PA, a boost PEC, and an H Full Bridge (HFB) single-phase inverter, this topology is typical in low power installations [3]. Fig. 7 shows the proposed topology, where: G is the radiation received by the PA, i_p is the PA current, v_p is the PA voltage, i_d is the current through the boost inductor (L_d), i_{Cp} is the current through the PA capacitor (C_p), r_d is the resistance associated with L_d, i_{Cd} is the current through the coupling capacitor between the boost and the HFB (C_d), i_{cd} is the current in the HFB DC side, v_{dc} is the voltage in the HFB DC side, i_a is the current in the HFB AC side and corresponds to the current in the inductor of the HFB AC side (L_a), v_{ac} is the voltage in the HFB AC side, i_z is the current of the AC side load (z), i_g is the current of the MG, and v_g is the voltage of the MG. D represents the duty cycle of the boost PEC power switch and Q_1 to Q_4 the duty cycles of the switches that make up the HFB.

1) PHOTOVOLTAIC ARRAY EMULATOR

The behavior of the PA is described by the logarithmic model used by the Keysight E4360A PA emulator [25]. This emulator is used to substitute real PA obtaining satisfactory results [26]–[31]. The model is shown in (1) in which: V_{oc} is the open circuit voltage, I_{sc} is the short circuit current, V_{mpp} is the maximum power point voltage, and I_{mpp} is the maximum power point current. The variables R_s, and N are also functions of the PA parameters (V_{oc}, V_{mpp}, I_{sc} and I_{mpp}) [25].

$$v_p = \frac{\frac{V_{oc} ln\left[2-\left(i_p/I_{sc}\right)^N\right]}{ln(2)} - R_s\left(i_p - I_{sc}\right)}{1 + \frac{R_s I_{sc}}{V_{oc}}} \tag{1}$$

To establish a dependency between the power of the GcRPVS and the behavior of the PA in the CHILE, the operation curves of the panels that make up the PA of the GcRPVS were analyzed [32]. Thus, the parameters on which the model of (1) depends on were related to the radiation received by the panel under standard conditions. Equations (2) to (4) present the relationships of the parameters V_{oc}, I_{sc} and the maximum power (M_p) with solar radiation, these equations present correlation coefficients (R^2) of 0.9989, ≈1, and ≈1, respectively

$$V_{oc} = 1.8572 ln\,(G) + 35.5459 \tag{2}$$
$$I_{sc} = 0.0097G - 0.0587 \tag{3}$$
$$M_p = 0.3758G - 4.8485 \tag{4}$$

Subsequently, the two geometric figures formed by two V-I curves were analyzed for different radiations. If the figure formed when the panel receives radiation G is denoted by S_G

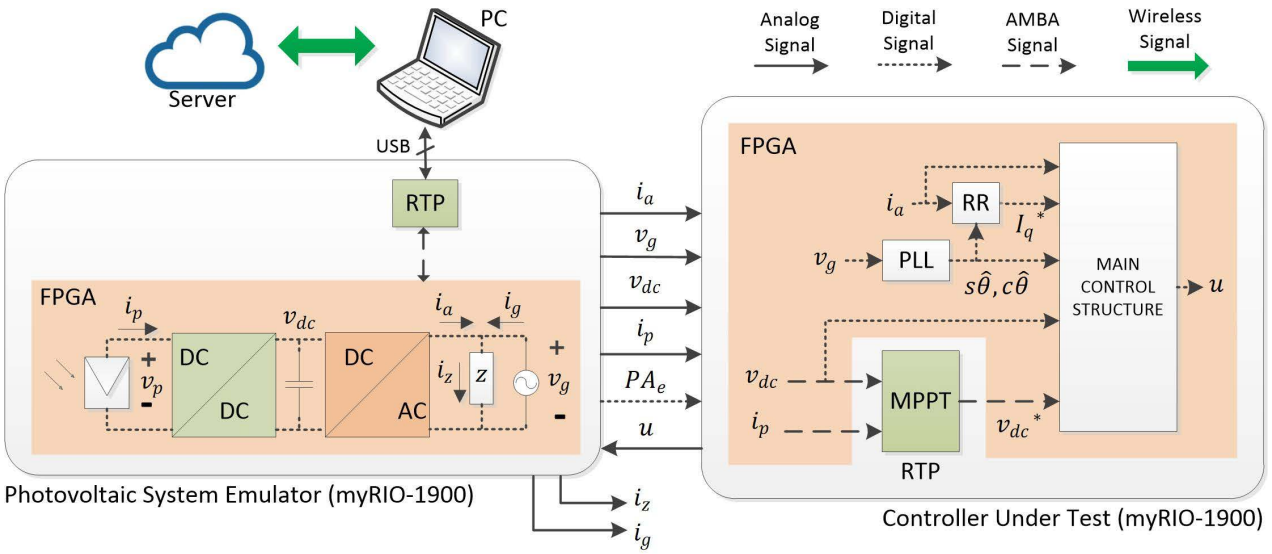

FIGURE 6. CHILE scheme.

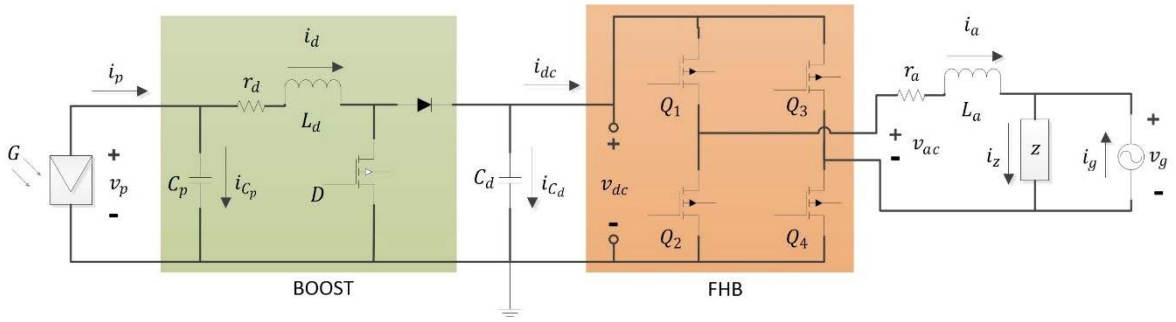

FIGURE 7. Topology of the GcRPVS.

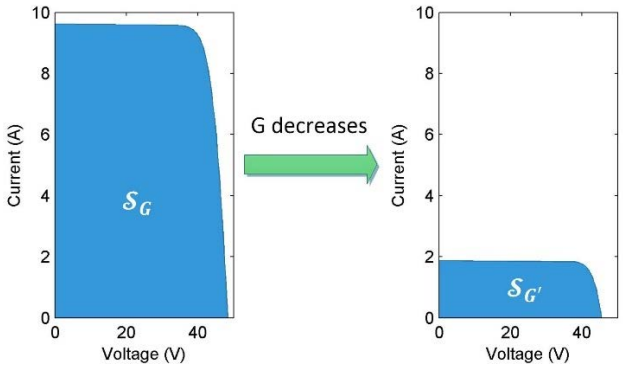

FIGURE 8. Comparison between V-I curves.

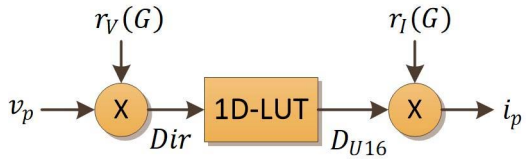

FIGURE 9. Photovoltaic array emulator.

and the figure formed when the panel receives radiation G' by $S_{G'}$, so that $G>G'$, it is observed that S_G is bigger than $S_{G'}$ as shown in Fig. 8.

To emulate the V-I curves, a one-dimensional lookup table (1D-LUT) was used with 1024 items U16 data type generated from (1) [33]–[35]. With a 1D-LUT only one V-I curve can be emulated; however, starting from the analysis of Fig. 8, this curve was scaled to generate V-I curves for different radiations. The panel voltage v_p was scaled so that its domain, from 0 to V_{oc}, corresponds to the addresses of the 1D-LUT, from 0 to 1023. Likewise, the data generated by the look up table was scaled so that its domain, from 0 to 65535, corresponds to i_p values from 0 to I_{sc}. This scaling was generated as shown in (5) and (6). Where Dir corresponds to the address of the 1D-LUT, D_{U16} corresponds to the data generated by the 1D-LUT, and $r_V\,(G)$ and $r_I\,(G)$ are proportionality factors that depend on G. The values of $V_{oc}\,(G)$ and $I_{sc}\,(G)$ are obtained with (2) and (3), while radiation G is obtained from (4) using the maximum power generated in the GcRPVS as input. The implementation of the PA emulator (PAE) is

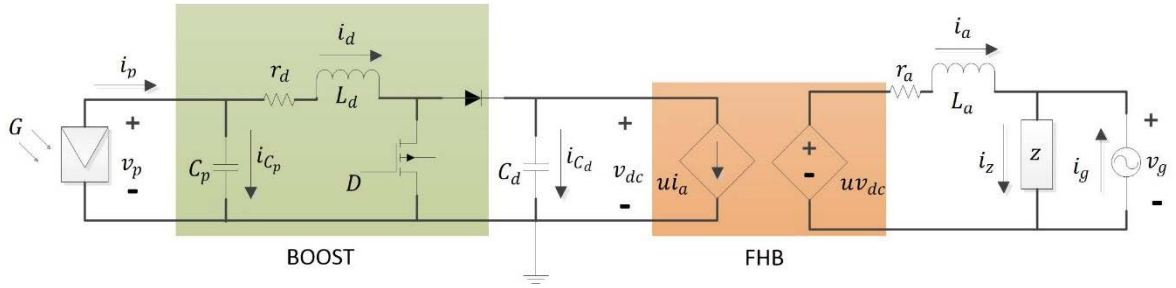

FIGURE 10. Reduced topology of the GcRPVS.

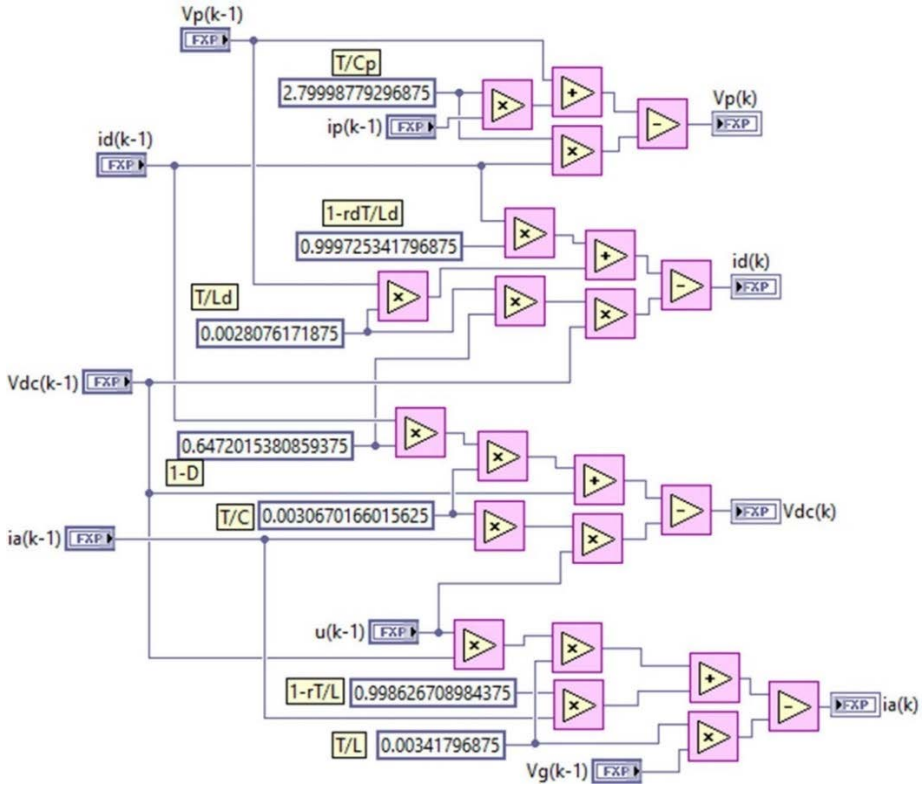

FIGURE 11. PEC emulator.

shown in Fig. 9. The factors $r_V\ (G)$ and $r_I\ (G)$ are calculated in the PC based on the power generated by the GcRPVS."

$$Dir = v_p \frac{1023}{V_{oc}\ (G)} = v_p r_V\ (G) \tag{5}$$

$$i_p = D_{U16} \frac{I_{sc}\ (G)}{65535} = D_{U16} r_I\ (G) \tag{6}$$

2) POWER ELECTRONIC CONVERTER

The PEC model describes the dynamics of the boost and the HFB and was presented as an averaged model. The switching signals of the switches Q_1 - Q_4 of the HFB presented in the topology of Fig. 7 are generated using the unipolar sinusoidal pulse width modulation (SPWM) technique. In this technique, the sinusoidal signal u from (7), (where m is the amplitude, α is the phase angle regarding v_g and $\omega = 2\pi f$ is the MG frequency) is compared with a triangular signal with frequency f_c significantly larger than f [36]. Since $f_c \gg f$, the average of the switching signals corresponds to

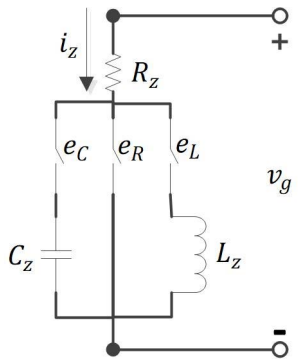

FIGURE 12. Load diagram.

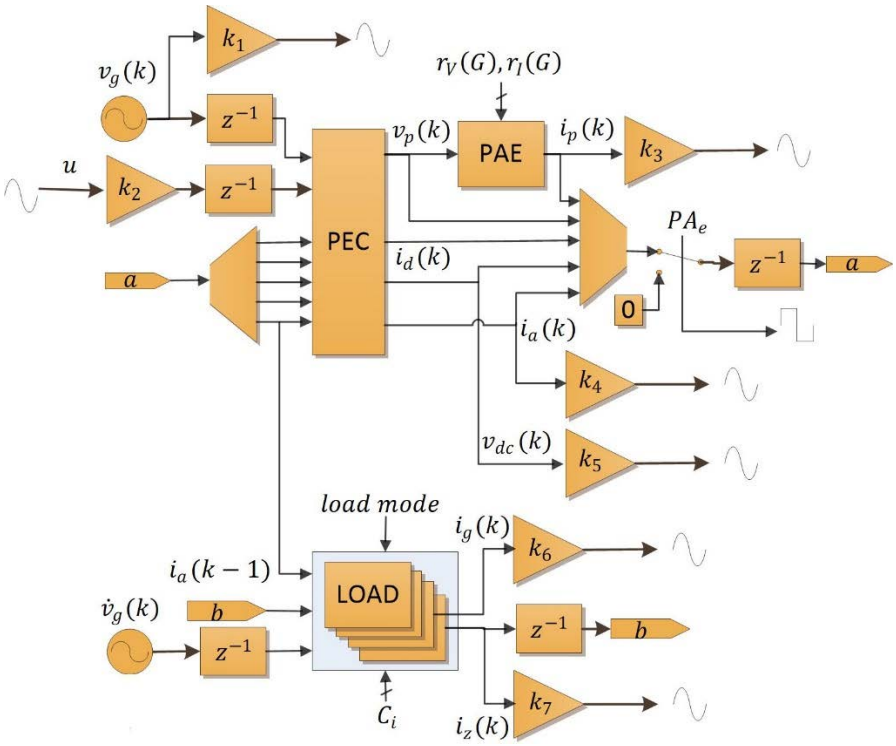

FIGURE 13. Implementation of the PVSE.

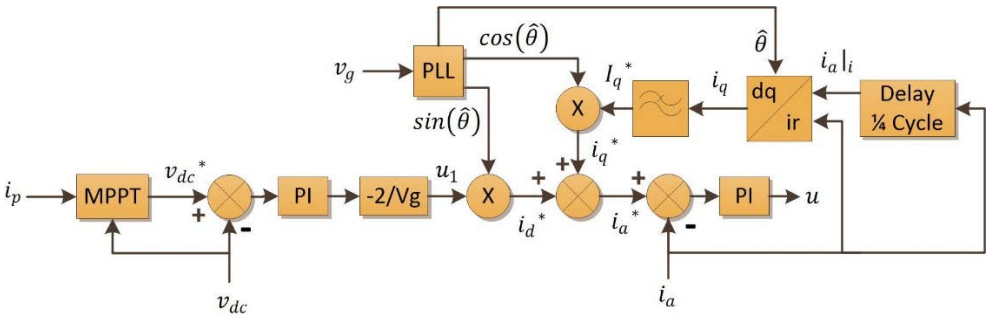

FIGURE 14. Controller diagram.

the modulating signal u [37]. Given this consideration, the HFB is replaced by two dependent sources so that $i_{dc} = ui_a$ and $v_{ac} = uv_{dc}$ [38]. These dependences are described by the topology shown in Fig. 10.

$$u = m\, sen(\omega t + \alpha) \tag{7}$$

From the diagram in Fig. 10 and applying Kirchof's laws to the loops and nodes that involve the inductors and capacitors, (8) and (9) were obtained for the boost [39] and (10) and (11) for the HFB. Finally, applying Kirchof's current law to the node that connects the AC side of the HFB, the AC load, and the MG, (12) was obtained.

$$v_p(k) = v_p(k-1) + \frac{T}{C_p} i_p(k-1) - \frac{T}{C_p} i_d(k-1) \tag{8}$$

$$i_d(k) = \left(1 - \frac{Tr_d}{L_d}\right) i_d(k-1) - \frac{T}{L_d}(1-D)\, v_{dc}(k-1) + \frac{T}{L_d} v_p(k-1) \tag{9}$$

$$v_{dc}(k) = v_{dc}(k-1) + \frac{T}{C_d}(1-D)\, i_d(k-1) - \frac{T}{C_d} u i_a(k-1) \tag{10}$$

$$i_a(k) = \left(1 - \frac{Tr_a}{L_a}\right) i_a(k-1) + \frac{T}{L_a} u v_{dc}(k-1) - \frac{T}{L_a} v_g(k-1) \tag{11}$$

$$i\_g(k) = i\_z(k) - i\_a(k) \tag{12}$$

The implementation of the elements that make up the CHILE was carried out using the software LabVIEW [40]. Fig. 11 shows the implementation in this environment of the PEC emulator (PECE) corresponding to (8) to (11).

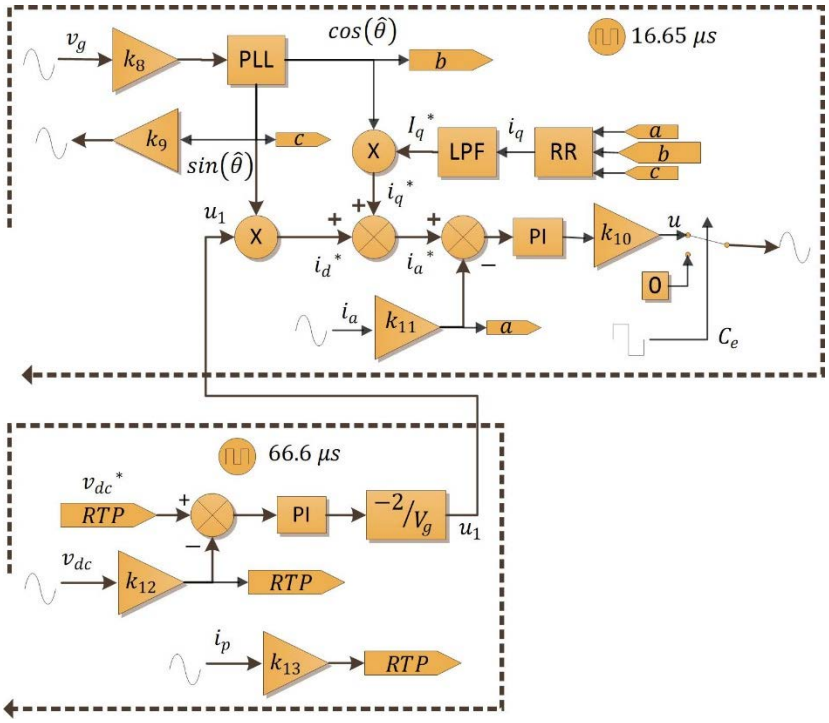

FIGURE 15. Controller implementation.

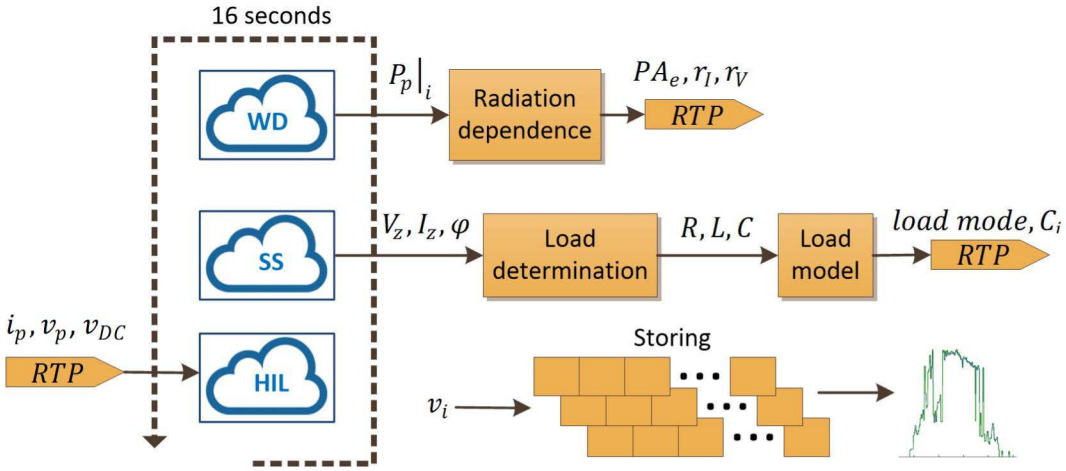

FIGURE 16. Implementation on the PC.

This figure shows the use of high-throughput blocks and fixed-point data type, these two aspects affect the performance and use of hardware resources of the emulator [41].

3) LOAD EMULATION

Fig. 12 shows the AC load diagram, which has four operating modes: "no load (I)," with switches e_C, e_R and e_L open; "R load (II)," with only the e_R switch closed; "R-C load (III)" with only the switch e_C closed and "R-L load (IV)" with only the e_L switch closed. By applying Kirchof's voltage law to the loop of Fig. 12, (13) was obtained, which describes the behavior of the load current i_z, for each operating mode.

$$i_z(k) = \begin{cases} 0 & ; I \\ \dfrac{v_g(k)}{R_z} & ; II \\ \left(1 - \dfrac{T}{R_z C_z}\right) i_z(k-1) + \dfrac{T}{R_z} \dot{v}_g(k-1) & ; III \\ \left(1 - \dfrac{TR_z}{L_z}\right) i_z(k-1) + \dfrac{T}{L_z} v_g(k-1) & ; IV \end{cases} \tag{13}$$

4) EMULATORS INTEGRATION

Fig. 13 shows the schematic diagram of the implementation of the PVSE that corresponds to the topology shown in Fig. 7. This emulator integrates the PAE described in section IV-A-1), the PECE shown in Fig. 11, and the load model presented in (13). This system is executed on the FPGA every 14 μs. To generate the variables at the moment $k-1$, shift registers represented as blocks z^{-1} were used. The load model was implemented in a case structure that determines the equation to solve based on the variable "load mode." The variables C_i correspond to the terms $1/R_z$, $1-T/(R_zC_z)$, T/R_z, $1-(TR_z)/L_z$, and T/L_z of (13). The variable PA_e gives a value of 0 to the signals v_p, i_p, i_d, i_a, and v_{dc} through a selector when the panel does not produce energy. The variables $r_V(G)$, $r_I(G)$, C_i, "load mode," and PA_e are determined in the PC and sent to the FPGA, where the topology was implemented, through the RTP of the myRIO. In this emulator, sinusoidal signals are also generated that emulate the behavior of the MG and its derivative. This emulator has 6 analog output signals that represent the variables v_g, i_p, i_a, v_{dc}, i_g, and i_z, and these are used for CHILE monitoring and interconnection with the CUT. It also has a digital signal corresponding to the variable PA_e and an analog input corresponding to the control signal u coming from the CUT. The constants k_1 to k_7 are used to normalize the analog signals.

B. CONTROLLER UNDER TEST

The control structure is composed of two parts, a perturb and observe controller for the MPPT and two nested loops with PI controllers for v_{dc} and i_a control [3], [42]. Fig. 14 shows the implemented controller with which the maximum power is extracted from the PA and the current injected into the MG, i_a, is generated in phase with it. The controller for the MPPT is based on the Hill Climbing algorithm to maximize the power generated by the PA through changes in the boost duty cycle [43], [44]. The algorithm implemented in this work maximizes the product of v_{dc} and i_p by modifying the value established for v_{dc}; since the boost operates with a fixed duty cycle. The reference signals $sin\left(\hat{\theta}\right)$ and $cos\left(\hat{\theta}\right)$ are generated by a Phase-Locked Loop (PLL) block type Park-PLL that is characterized by having a relatively fast transient response and high rejection to disturbances [45]. The reactive current reference I_q^* is calculated using a quarter cycle delay and the Park transformation; in addition, the reference obtained by the Park transformation is filtered with a first order low pass filter.

Fig. 15 shows the CUT implementation, it was divided into two while loops. The first one has an execution time of 16.65 μs and integrates the PLL, the calculation of the reactive current reference RR, the low pass filter LPF, and the inner PI. This loop has as analog inputs the signals v_g and i_a and a digital input. C_e that comes from PSE ($C_e = PA_e$). Furthermore, an analog control signal u is generated in this loop. The second block has an execution time of 66.6 μs, it integrates the outer PI and communicates with the RTP

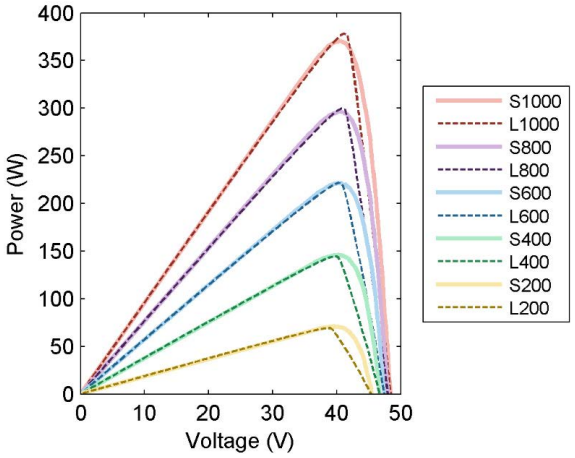

FIGURE 17. Comparison between the V-P curves.

where the controller for the MPPT was implemented. This loop has as analog inputs the signals i_p and v_{dc} coming from the PSE. The constants k_8 to k_{13} are used to normalize the analog signals.

C. PC IMPLEMENTATION

The PC performs three functions: it establishes communication with the database in the cloud, it determines constants that allow the CHILE to replicate the behavior of GcRPVS and AC loads, and it provides a user interface to observe the behavior of the CHILE. The PC makes a request every 16 seconds to the channels corresponding to the web driver (WD), the SS and the CHILE (HIL). From the WD channel, the data corresponding to the power generated in the GcRPVS $P_p \mid i$ is extracted and using (4) to (6) the variables G, $r_V(G)$, and $r_I(G)$ are determined and sent to the FPGA through the RTP. From the SS channel, the RMS voltage of the load V_z, the RMS current of the load I_z, and the phase angle between these two signals φ are extracted, with the data the values of R, and L or C are determined, using (14) to (16) [46]. Subsequently, from (13), the terms C_i and load model are calculated and sent to the FPGA through the RTP. The variables i_p, v_p, and v_{dc} are generated in the CHILE, sent to the PC through RTP and later to the cloud database. Finally, the relevant operation variables obtained from the cloud or generated in the CHILE are stored in registers and displayed graphically in a user interface developed in LabVIEW. These variables are solar radiation, panel current, v_{dc}, voltage, load power, load phase angle, GcRPVS power, and PA power in the CHILE. Fig. 16 shows the representation of the implementation on the PC.

$$R = \begin{cases} \dfrac{V_g}{I}\left[1 - \dfrac{1}{\sqrt{tan^2(90-\emptyset)+1}}\right] & 0 \le \emptyset < 90 \\ \dfrac{V_g}{I}\left[1 - \dfrac{1}{\sqrt{\dfrac{1}{tan^2(-\emptyset)}+1}}\right] & -90 < \emptyset \le 0 \end{cases} \tag{14}$$

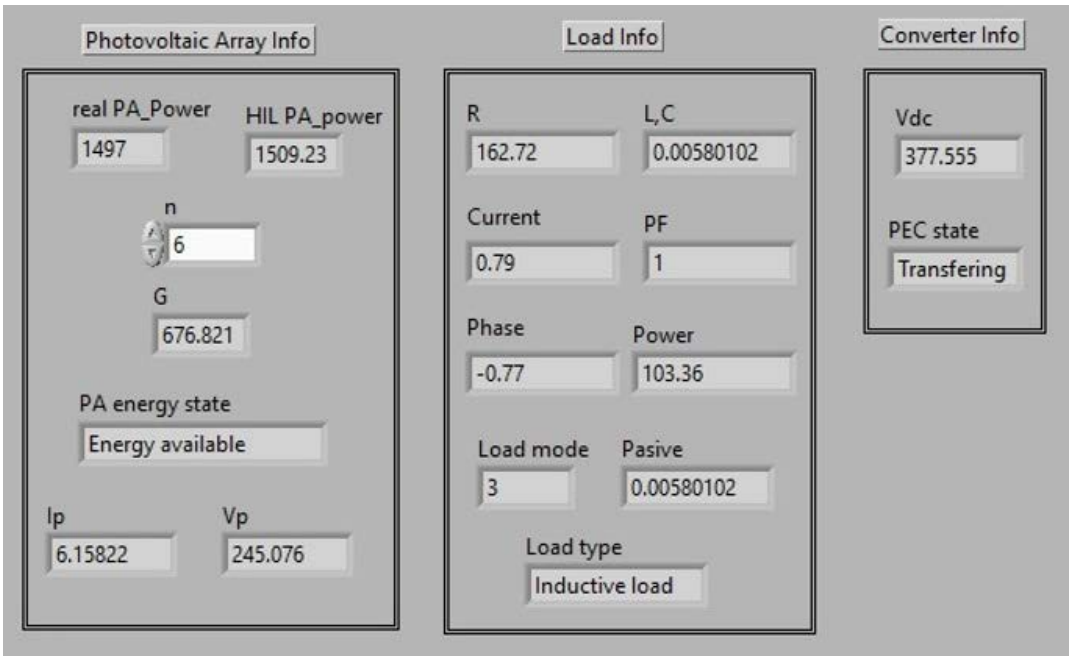

FIGURE 18. LabVIEW interface.

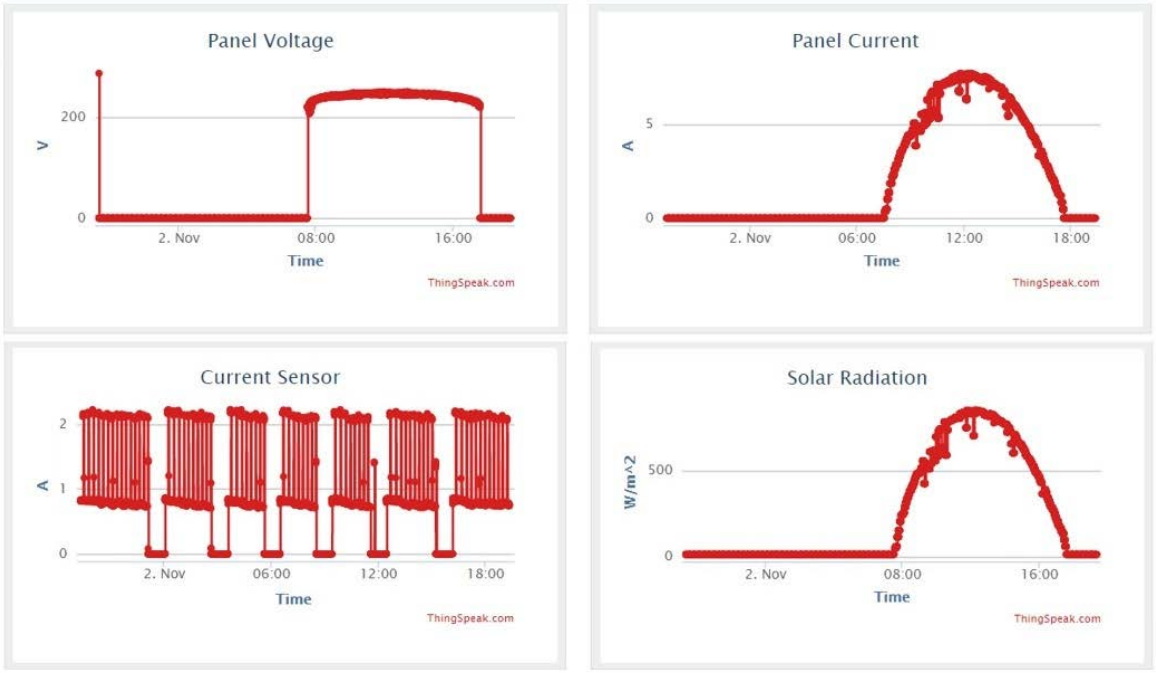

FIGURE 19. ThingSpeak charts.

$$C = \frac{1}{Rw} tan\,(90 - \emptyset) \tag{15}$$

$$L = \frac{R}{w} tan\,(-\emptyset) \tag{16}$$

V. RESULTS

Fig. 17 shows a comparison between the V-P curves presented by the supplier of the panels in [32] and the curves generated with the methodology presented in section IV-A-1) for different radiations. The curves identified by the names S200 to S1000 correspond to the graphs presented by the supplier in [32] for radiation from 200 to 1000 W/m^2, respectively, on the other hand, the curves identified as L200 to L1000 correspond to the curves generated by scaling the 1D-LUT for the same radiation values. In comparison with the manufacturer's curves, with the methodology used in this

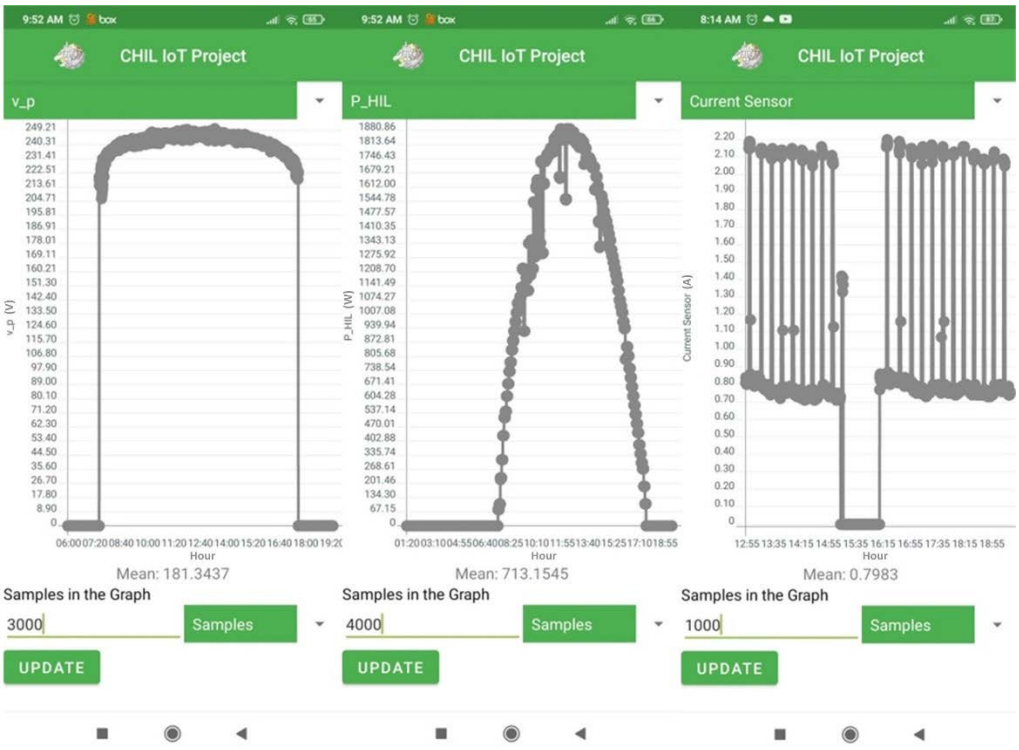

FIGURE 20. APP Chartviews.

research, an absolute error was obtained for the maximum power of 7.3 W, 2.9 W, 0.2 W, -1.3 W and -1.5 W for radiation of 1000 W/m2, 800 W/m2, 600 W/m2, 400 W/m2, and 200 W/m2, respectively, in terms of relative error these values represent variations of 0.02%, 0.001%, 8 × 10.4%, -0.001%, and -0.02%.

To validate the behavior of the CHILE, an experiment lasting 24 hours was carried out, during which the behavior of GcRPVS was reproduced. The structure of the CHILE allows the user to monitor it on the site where it is located and remotely through the Android application or by directly accessing the ThingSpeak server site. For the monitoring of the emulator on the site, a graphical interface was developed in LabVIEW, in which the user can observe specifically the value of the most relevant variables of the system with an update rate of 500 ms. As it's shown in Fig. 18 variables that user can observe in the interface are: from the PA, the power of the GcRPVS (real PA Power), the power produced by the PA in the CHILE (HIL PA Power), the solar radiation that produces this power (G), the state of the energy in the PA (''PA energy available'' when energy is available or ''No energy available'' when the panels do not generate energy), the PA current (i_p) and the PA voltage (v_p). In addition, in this system the user can define the number of panels (n) of 370 W connected in series that make up the PA. From the load, the value of R, the value of L or C, as the case may be, the RMS value of its current, the power factor, the phase angle, the apparent power and the load mode that takes the values of ''No load,'' ''Resistive load,'' ''Inductive Load,'' and ''Capacitive load.'' Finally, from the PEC, the DC voltage and the status of the PEC (''Transferring'' which indicates that the PA generates energy and this is transferred to the MG and ''Waiting'' when the PA does not generate energy and therefore the PEC is disconnected). In this graphical interface it is also possible to visualize the temporal evolution of the solar radiation, the panel current, the panel voltage, the v_{dc} voltage, the load power, the load phase angle, the GcRPVS power and the panel power in the CHILE.

Another option that the user has for monitoring the iCHIL platform is to enter the ThingSpeak server site, in this case the five channels described in section III-C can be accessed and the temporal evolution of the variables can be viewed with a resolution of 16 s. Fig. 19 shows a summary of the graphs of different channels that are displayed in ThingSpeak for the experiment carried out. Specifically, the responses of the PA voltage, the PA current, the load current and the solar radiation are observed.

Also, the user can monitor the behavior of the iCHIL platform through the developed APP. The results obtained in this aspect are shown in Fig. 20. This figure illustrates the panel voltage, the panel power in the CHILE, and the load current. In the APP, the user defines the variable to be displayed, as well as the number of data being plotted. To determine the response time of the server to an HTTP request, both generated in CHILE and in the APP, this parameter was measured during the experiment, obtaining that on average,

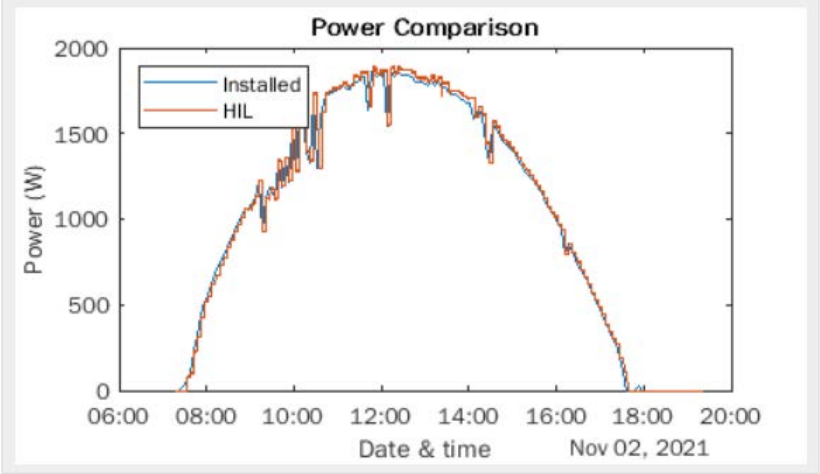

FIGURE 21. Comparison between the powers.

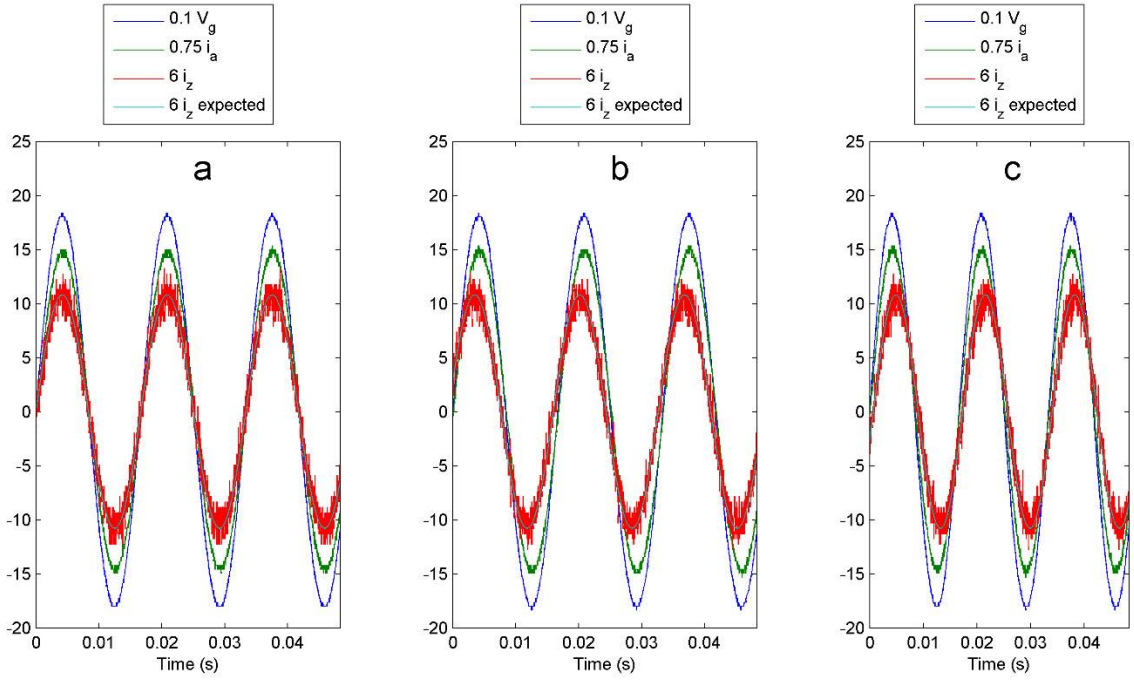

FIGURE 22. Behavior of i_a and i_z.

the server takes 441.9 ms to respond, likewise no data loss was observed.

The iCHIL platform, in addition to providing the user with a communications network based on IoT that allows him to monitor the temporal evolution of the most relevant variables of the PVS remotely, has the purpose of reproducing in real time the behavior of the GcRPVS and with it validate the functionality of controllers for the MPPT and the interconnection with the MG. Fig. 21 shows a comparison between the power generated by the GcRPVS and the power generated by the PAE, where an adequate reproduction of the behavior of the PA and a correct operation of the MPPT controller are verified. Compared to the power generated by the GcRPVS, the power of the PAE presents an absolute mean error of 9.1 W and a relative mean error of 0.42%.

Finally, Fig. 22 shows the results obtained for the load current (i_z) and the current that the inverter injects into the MG (i_a) with loads a) resistive, b) capacitive, and c) inductive. These currents are compared with the MG voltage (v_g) to evidence the compensation of the inverter controller for the reactive current and the correct reproduction of the behavior of the load. The current load generated by the emulator presented an absolute mean error of 11.5 mA, 4.9 mA and 13.6 mA compared to the expected current, for cases a), b) and c), respectively. The relative error present in this variable was not evaluated point by point due to the zero crossings

that make it tend to infinity, however, if its amplitude is taken as a reference value, this variable presents relative errors of 0.64%, 0.27% and 0.75% for cases a), b) and c), respectively.

VI. CONCLUSION

The methodology used to emulate the PA curves under different radiation conditions generates satisfactory results presenting a relative error for the maximum power of between 8×10^{-4} and 0.02%. Although this methodology does not accurately reproduce the curves presented by the supplier in its data sheet [32], the comparison made in the results section shows a satisfactory similarity. The proposed methodology uses a single 1D-LUT, this significantly reduces the use of development board resources and allows this methodology to be applied with generic hardware with relatively few features; for example, on hardware where the use of a multidimensional LUT is not available. Although the PA curves generated in the CHILE are always assumed under standard conditions, the comparison between the maximum power generated in the GcRPVS and that generated in the CHILE, shown in the results section, shows that this methodology allows to emulate a dynamic behavior of the panel that satisfactorily approximates its real behavior.

The results obtained demonstrate the correct functioning of the iCHIL platform. The comparative graph between the power generated in the GcRPVS and that generated in the iCHIL platform shows the ability of the CHILE to reproduce the behavior of the PA and the functionality of the controller for the implemented MPPT. On the other hand, the comparison between the MG voltage and the load current on the platform shows that the CHILE satisfactorily reproduces the behavior of the load. These results together with the IoT network, which provides the information for the emulator to reproduce the behavior of the PA and the load in real time, make the platform a tool with which controllers can be validated under realistic scenarios using the CHIL technique. In this way it is possible to evaluate the performance of controllers intended for real photovoltaic system applications without the investment that purchasing a system for testing implies. Another economic advantage of this platform has to do with time. With the use of the CHIL technique, different weather conditions, under which a controller is tested to determine the correct functioning could be emulated at any instant without the need for these conditions to occur naturally in the environment.

The technique proposed for the intercommunication of the iCHIL components, through HTTP requests to the ThingSpeak server, represented a communication without data loss in the experiment that was carried out, so this alternative is considered reliable for this application. However, the average response time of the server is high compared to studies like [20], where it is 25 ms. Despite this, the response time of the server does not affect the sampling time of the variables, which in the case of GcRPVS is 5 minutes, comparable to those presented in [15] and [16] for a similar application. In the case of the load, the sampling time is 16 s, so the server response time consumes only 2.5% of the period between requests. This latency is due to the fact that the observed load does not have fast dynamics. If, on the other hand, a reduction in the response time of the server is required, the use of the HTTP protocol, as proposed in this study, might not be enough, an alternative to this could be the use of the MQTT protocol used in studies such as [12], [13], [15] and [16].

In this research, the platform was validated by testing a controller for the PVS interconnection that integrates a control for the MPPT based on the Hill Climbing algorithm and a controller for the synchronization of the current generated in the PEC with the MG composed of PI controllers in cascade, however, the physical structure of the platform allows not only this controller to be verified, this feature makes the platform useful for the validation of practically any controller, either for the MPPT or for the interconnection with the MG. This assertion is confirmed considering that the PVS CHILE connects with the controller using analog inputs and outputs and was embedded independently of the controller, so that it is not necessary to modify the emulator to integrate a different controller. Another characteristic that makes the platform versatile is that the behavior of the AC load is generated from the monitoring of a real load, so that if it is required to test the system with a specific load, it is only necessary to connect the SS to it and with this its behavior will be reflected in the CHILE. Something similar applies to the installed PVS. If there is access to the online information of an installed PVS, it can be emulated in the CHILE with the IoT network proposed in this study.

The iCHIL platform for this investigation was developed using low-cost generic hardware, compared to commercial platforms dedicated to the implementation of HIL simulations. Also, the mathematical models were embedded using a high-level language, this represents a faster and more reproducible implementation process compared to the use of hardware description languages. These characteristics together make this platform reproducible by other researchers. The platform represents a research infrastructure for the development of research related to the study of controllers for interconnected PVS, so its reproducibility could promote the development of research in this field.

The implemented IoT network allows the platform not only to reproduce the behavior of the PVS and the AC load under realistic scenarios, but also, together with the developed mobile application, it allows the user to remotely monitor the behavior of the system. Considering the variations observed in the power in the GcRPVS and the AC load current, the 16 s update rate of the cloud database provides enough information to describe, graphically, the temporal evolution of the variables of interest without losing detail of their behavior.

The correct reproduction of the behavior of the system is mainly due to the fact that the monitored load does not have fast dynamics. However, in the case of loads with a more dynamic behavior, the proposed sampling rate would not be enough, as well as the response time of the server. This problem could be solved in the future by integrating

the MQTT protocol and load behavior pattern recognition in the FOG layer, the research presented in [11] supports the advantages of this approach. Another option to solve this problem could be to implement a VPN tunnel with the UDP protocol, in [20] this alternative produces a latency time of just 12.5 ms between two locations separated by a distance of 1000 km.

REFERENCES

[1] M. H. Shubbak, "Advances in solar photovoltaics: Technology review and patent trends," *Renew. Sustain. Energy Rev.*, vol. 115, Nov. 2019, Art. no. 109383, doi: 10.1016/j.rser.2019.109383.

[2] R. Khezri, A. Mahmoudi, and H. Aki, "Optimal planning of solar photovoltaic and battery storage systems for grid-connected residential sector: Review, challenges and new perspectives," *Renew. Sustain. Energy Rev.*, vol. 153, Jan. 2022, Art. no. 111763, doi: 10.1016/j.rser.2021.111763.

[3] K. Zeb, I. Khan, W. Uddin, M. A. Khan, P. Sathishkumar, T. D. C. Busarello, I. Ahmad, and H. J. Kim, "A review on recent advances and future trends of transformerless inverter structures for single-phase grid-connected photovoltaic systems," *Energies*, vol. 11, no. 8, p. 1968, Jul. 2018, doi: 10.3390/en11081968.

[4] K. Padmanathan, U. Govindarajan, V. K. Ramachandaramurthy, S. O. Selvi, and B. Jeevarathinam, "Integrating solar photovoltaic energy conversion systems into industrial and commercial electrical energy utilization—A survey," *J. Ind. Inf. Integr.*, vol. 10, pp. 39–54, Jun. 2018, doi: 10.1016/j.jii.2018.01.003.

[5] F. Ebe, B. Idlbi, D. Stakic, S. Chen, C. Kondzialka, M. Casel, G. Heilscher, C. Seitl, R. Bründlinger, and T. Strasser, "Comparison of power hardware-in-the-loop approaches for the testing of smart grid controls," *Energies*, vol. 11, no. 12, p. 3381, Dec. 2018, doi: 10.3390/en11123381.

[6] M. H. Syed, E. Guillo-Sansano, Y. Wang, S. Vogel, P. Palensky, G. M. Burt, Y. Xu, A. Monti, and R. Hovsapian, "Real-time coupling of geographically distributed research infrastructures: Taxonomy, overview, and real-world smart grid applications," *IEEE Trans. Smart Grid*, vol. 12, no. 2, pp. 1747–1760, Mar. 2021, doi: 10.1109/TSG.2020.3033070.

[7] R. Salcedo, E. Corbett, and C. Smith, "Banshee distribution network benchmark and prototyping platform for hardware-in-the-loop integration of microgrid and device controllers," *J. Eng.*, vol. 2019, no. 8, pp. 5365–5373, Apr. 2019, doi: 10.1049/joe.2018.5174.

[8] V. Samano-Ortega, H. Rodriguez-Estrada, E. Rodríguez-Segura, J. Padilla-Medina, J. Aguilera-Alvarez, and J. Martinez-Nolasco, "Power sharing control in a grid-tied DC microgrid: Controller hardware in the loop validation," *Appl. Sci.*, vol. 11, no. 19, p. 9295, Oct. 2021, doi: 10.3390/app11199295.

[9] V. Samano-Ortega, A. Padilla-Medina, M. Bravo-Sanchez, E. Rodriguez-Segura, A. Jimenez-Garibay, and J. Martinez-Nolasco, "Hardware in the loop platform for testing photovoltaic system control," *Appl. Sci.*, vol. 10, no. 23, p. 8690, Dec. 2020, doi: 10.3390/app10238690.

[10] B. Babes, F. Albalawi, N. Hamouda, S. Kahla, and S. S. M. Ghoneim, "Fractional-fuzzy PID control approach of photovoltaic-wire feeder system (PV-WFS): Simulation and HIL-based experimental investigation," *IEEE Access*, vol. 9, pp. 159933–159954, 2021, doi: 10.1109/ACCESS.2021.3129608.

[11] R. Rajavel, S. K. Ravichandran, K. Harimoorthy, P. Nagappan, and K. R. Gobichettipalayam, "IoT-based smart healthcare video surveillance system using edge computing," *J. Ambient Intell. Humanized Comput.*, vol. 13, no. 6, pp. 3195–3207, Jun. 2022, doi: 10.1007/s12652-021-03157-1.

[12] M. Elsisi, M. Q. Tran, K. Mahmoud, D. E. A. Mansour, M. Lehtonen, and M. M. Darwish, "Effective IoT-based deep learning platform for online fault diagnosis of power transformers against cyberattacks and data uncertainties," *Measurement*, vol. 190, Feb. 2022, Art. no. 110686, doi: 10.1016/j.measurement.2021.110686.

[13] M.-Q. Tran, M. Elsisi, M.-K. Liu, V. Q. Vu, K. Mahmoud, M. M. F. Darwish, A. Y. Abdelaziz, and M. Lehtonen, "Reliable deep learning and IoT-based monitoring system for secure computer numerical control machines against cyber-attacks with experimental verification," *IEEE Access*, vol. 10, pp. 23186–23197, 2022, doi: 10.1109/ACCESS.2022.3153471.

[14] Y. Kabalci, E. Kabalci, S. Padmanaban, J. B. Holm-Nielsen, and F. Blaabjerg, "Internet of Things applications as energy Internet in smart grids and smart environments," *Electronics*, vol. 8, no. 9, p. 972, Aug. 2019, doi: 10.3390/electronics8090972.

[15] P. de Arquer Fernández, M. Á. Fernández Fernández, J. L. Carús Candás, and P. Arboleya Arboleya, "An IoT open source platform for photovoltaic plants supervision," *Int. J. Electr. Power Energy Syst.*, vol. 125, Feb. 2021, Art. no. 106540, doi: 10.1016/j.ijepes.2020.106540.

[16] R. I. S. Pereira, S. C. S. Jucá, and P. C. M. Carvalho, "IoT embedded systems network and sensors signal conditioning applied to decentralized photovoltaic plants," *Measurement*, vol. 142, pp. 195–212, Aug. 2019, doi: 10.1016/j.measurement.2019.04.085.

[17] H. K. Ahn and N. Park, "Deep RNN-based photovoltaic power short-term forecast using power IoT sensors," *Energies*, vol. 14, no. 2, p. 436, Jan. 2021, doi: 10.3390/en14020436.

[18] A. Valibeygi, R. A. de Callafon, M. Stanovich, M. S. K. Schoder, J. L. I. Leonard, S. Chatterjee, and R. Meeker, "Microgrid control using remote controller hardware-in-the-loop over the internet," in *Proc. IEEE Power Energy Soc. Innov. Smart Grid Technol. Conf. (ISGT)*, Washington, DC, USA, Feb. 2018, pp. 1–5, doi: 10.1109/ISGT.2018.8403345.

[19] S. Vogel, H. T. Nguyen, M. Stevic, T. V. Jensen, K. Heussen, V. S. Rajkumar, and A. Monti, "Distributed power hardware-in-the-loop testing using a grid-forming converter as power interface," *Energies*, vol. 13, no. 15, p. 3770, Jul. 2020, doi: 10.3390/en13153770.

[20] E. Bompard, S. Bruno, A. Cordoba-Pacheco, C. Diaz-Londono, G. Giannoccaro, M. La Scala, A. Mazza, and E. Pons, "Latency and simulation stability in a remote power hardware-in-the-loop cosimulation testbed," *IEEE Trans. Ind. Appl.*, vol. 57, no. 4, pp. 3463–3473, Aug. 2021, doi: 10.1109/TIA.2021.3082506.

[21] S. Kochanneck, I. Mauser, K. Phipps, and H. Schmeck, "Hardware-in-the-loop co-simulation of a smart building in a low-voltage distribution grid," in *Proc. IEEE PES Innov. Smart Grid Technol. Conf. Eur. (ISGT-Europe)*, Oct. 2018, pp. 1–6, doi: 10.1109/ISGTEurope.2018.8571746.

[22] M. Thornton, M. Motalleb, H. Smidt, J. Branigan, P. Siano, and R. Ghorbani, "Internet-of-Things hardware-in-the-loop simulation architecture for providing frequency regulation with demand response," *IEEE Trans. Ind. Informat.*, vol. 14, no. 11, pp. 5020–5028, Nov. 2018, doi: 10.1109/TII.2017.2782885.

[23] R. Ayop and C. W. Tan, "A comprehensive review on photovoltaic emulator," *Renew. Sustain. Energy Rev.*, vol. 80, pp. 430–452, Dec. 2017, doi: 10.1016/j.rser.2017.05.217.

[24] (May 2016). *User Guide and Specifications NI myRIO-1900*. National Instruments. [Online]. Available: https://www.ni.com/pdf/manuals/376047c.pdf

[25] *Keysight Technologies Series E4360 Modular Solar Array Simulator*. Keysight Technolagy. Budd Lake, NJ, USA. Accessed: Dec. 8, 2018. [Online]. Available: http://literature.cdn.keysight.com/litweb/pdf/E4360-90001.pdf

[26] Y. Pan, Y. Yang, and F. Blaabjerg, "Distributed control of islanded series PV-battery-hybrid systems with low communication burden," in *Proc. IEEE 11th Int. Symp. Power Electron. Distrib. Gener. Syst. (PEDG)*, Dubrovnik, Croatia, Sep. 2020, pp. 315–321, doi: 10.1109/PEDG48541.2020.9244482.

[27] K. Kanathipan, R. Emamalipour, and J. Lam, "A single-switch high-gain PV microconverter with low-switch-voltage-to-high-voltage-bus ratio," *IEEE Trans. Power Electron.*, vol. 35, no. 9, pp. 9530–9540, Sep. 2020, doi: 10.1109/TPEL.2020.2974207.

[28] Y. Pan, A. Sangwongwanich, Y. Yang, and F. Blaabjerg, "A series inter-harmonic filter for cascaded H-bridge PV inverters," in *Proc. IEEE Energy Convers. Congr. Expo. (ECCE)*, Detroit, MI, USA, Oct. 2020, pp. 341–346, doi: 10.1109/ECCE44975.2020.9235745.

[29] P. Upadhyay, S. Pulipaka, M. Sharma, and R. Kumar, "A proposed maximum power point operating strategy for photovoltaic applications using monthly irradiance estimates," *Sol. Energy*, vol. 141, pp. 266–277, Jan. 2017, doi: 10.1016/j.solener.2016.11.046.

[30] Z. Lin, W. Xie, M. Dong, and J. Lan, "Research of S3MPR engineering application on space power sources," in *Proc. IEEE 4th Inf. Technol., Netw., Electron. Autom. Control Conf. (ITNEC)*, Chongqing, China, Jun. 2020, pp. 817–823, doi: 10.1109/ITNEC48623.2020.9084923.

[31] D. Fernandes, R. Almeida, T. Guedes, A. J. Sguarezi Filho, and F. F. Costa, "State feedback control for DC-photovoltaic systems," *Electr. Power Syst. Res.*, vol. 143, pp. 794–801, Feb. 2017, doi: 10.1016/j.epsr.2016.08.037.

[32] (2019). *SRP-6MA-DG Series 6 Inch 72 Cells 355-370W*. Seraphim Solar System. [Online]. Available: https://www.seraphim-energy.com/wp-content/uploads/download/Dual-Glass-Module-72-Mono-Perc.pdf
[33] S. Jenkal, M. Kourchi, A. Rachdy, M. Ajaamoum, O. Oussalem, and H. Idadoub, "Design and implementation of an agilent-based platform for PV feature generator based on LUT tables," *Mater. Today: Proc.*, vol. 24, pp. 95–99, 2020, doi: 10.1016/j.matpr.2019.07.687.
[34] C. Levis, C. O'Loughlin, T. O'Donnell, and M. Hill, "A comprehensive state-space model of two-stage grid-connected PV systems in transient network analysis," *Int. J. Electr. Power Energy Syst.*, vol. 110, pp. 441–453, Sep. 2019, doi: 10.1016/j.ijepes.2019.03.032.
[35] M. Balato, L. Costanzo, D. Gallo, C. Landi, M. Luiso, and M. Vitelli, "Design and implementation of a dynamic FPAA based photovoltaic emulator," *Solar Energy*, vol. 123, pp. 102–115, Jan. 2016, doi: 10.1016/j.solener.2015.11.006.
[36] J. C. Sanabria Rojas, D. M. Barrera Leguizamon, D. A. Bautista Lopez, and F. R. Jimenez Lopez, "Simulation of the model, design and control of a current source inverter with unipolar SPWM modulation," in *Proc. IEEE 15th Brazilian Power Electron. Conf. 5th IEEE Southern Power Electron. Conf. (COBEP/SPEC)*, Santos, Brazil, Dec. 2019, pp. 1–5, doi: 10.1109/COBEP/SPEC44138.2019.9065891.
[37] Y. Peng, W. Sun, and F. Deng, "Internal model principle method to robust output voltage tracking control for single-phase ups inverters with its SPWM implementation," *IEEE Trans. Energy Convers.*, vol. 36, no. 2, pp. 841–852, Jun. 2021, doi: 10.1109/TEC.2020.3030894.
[38] O. Gonzalez, J. Perez-Ramirez, and J. A. Beristain, "Photovoltaic power injection to the grid with reactive power and harmonic compensation using a simple h bridge converter," in *Proc. IEEE Workshop Power Electron. Power Quality Appl. (PEPQA)*, Bogota, Colombia, Jun. 2015, pp. 1–7, doi: 10.1109/PEPQA.2015.7168246.
[39] Y. Shen, Z. Qin, and H. Wang, "Modeling and control of DC–DC converters," in *Control of Power Electronic Converters and Systems*. Cambridge, MA, USA: Academic, 2018, pp. 69–92. [Online]. Available: https://www.sciencedirect.com/science/article/pii/B9780128052457000032
[40] L. Estrada, N. Vázquez, J. Vaquero, Á. de Castro, and J. Arau, "Real-time hardware in the loop simulation methodology for power converters using LabVIEW FPGA," *Energies*, vol. 13, no. 2, p. 373, Jan. 2020, doi: 10.3390/en13020373.
[41] (Feb. 2014). *NI LabVIEW High-Performance FPGA Developer's Guide*. National Instruments. [Online]. Available: https://www.ni.com/es-mx/support/documentation/supplemental/13/the-ni-labview-high-performance-fpga-developer-s-guide.html
[42] F. Liu, Y. Kang, Y. Zhang, and S. Duan, "Comparison of P&O and Hill climbing MPPT methods for grid-connected PV converter," in *Proc. 3rd IEEE Conf. Ind. Electron. Appl.*, Singapore, Jun. 2008, pp. 804–807, doi: 10.1109/ICIEA.2008.4582626.
[43] M. I. Bahari, P. Tarassodi, Y. M. Naeini, A. K. Khalilabad, and P. Shirazi, "Modeling and simulation of Hill climbing MPPT algorithm for photovoltaic application," in *Proc. Int. Symp. Power Electron., Electr. Drives, Autom. Motion (SPEEDAM)*, Capri, Italy, Jun. 2016, pp. 1041–1044, doi: 10.1109/SPEEDAM.2016.7525990.
[44] H. Palahalli, Y. Huo, and G. Gruosso, "Real time simulation of photovoltaic system using FPGA," in *Proc. Int. Symp. Power Electron., Electr. Drives, Autom. Motion (SPEEDAM)*, Amalfi, Italy, Jun. 2018, pp. 865–870, doi: 10.1109/SPEEDAM.2018.8445288.
[45] Y. Han, M. Luo, X. Zhao, J. M. Guerrero, and L. Xu, "Comparative performance evaluation of orthogonal-signal-generators-based single-phase PLL algorithms—A survey," *IEEE Trans. Power Electron.*, vol. 31, no. 5, pp. 3932–3944, May 2016, doi: 10.1109/TPEL.2015.2466631.
[46] T. J. Davies, *Newnes Circuit Calculations Pocket Book: With Computer Programs*. Amsterdam, The Netherlands: Elsevier, 1992. [Online]. Available: https://www.sciencedirect.com/book/9780750601955/newnes-circuit-calculations-pocket-book

VÍCTOR SÁMANO-ORTEGA received the B.S. degree in mechatronics engineering and the M.S. degree in mechanical engineering from the Technological Institute of Celaya, Guanajuato, Mexico, in 2017 and 2019, respectively, where he is currently pursuing the Ph.D. degree in engineering sciences. His research interests include intelligent control, direct current microgrids, and energy systems emulators.

HUGO MÉNDEZ-GUZMÁN received the B.Sc. and M.Sc. degrees in electronic engineering from the Ciudad Guzman Institute of Technology, Jalisco, Mexico, in 2007 and 2012, respectively. He is currently pursuing the Ph.D. degree with the Celaya Institute of Technology. His research interests include the Internet of Things, smart farming, image processing, and artificial intelligence.

JOSÉ PADILLA-MEDINA was born in Iguala, Guerrero, Mexico, in April 1969. He received the degree in electrical engineering from the Technological Institute of Celaya, Mexico, in 1991, the M.S. degree in electrical engineering from Guanajuato University, in 1995, the Ph.D. degree in science (optics) from the Centro de Investigaciones en Óptica, in 2002. He is currently a Teacher and a Researcher with the Department of Electronics Engineering, Technological Institute of Celaya. His research interests include study of biological tissues, visual perception, applications of fuzzy logic, and image processing.

JUAN AGUILERA-ÁLVAREZ received the master's degree in mechanical science from the Tecnológico Nacional de México en Celaya, in 2016, where he is currently pursuing the Ph.D. degree working on project in medical application. His research interests include programming, web applications, signal processing, the IoT analytics, predictive computing, automation systems, and 3D printing.

CORAL MARTÍNEZ-NOLASCO received the degree in electronic engineering from the Instituto Tecnológico de Ciudad Guzmán, Jalisco, Mexico, in 2009, and the Master of Science degree in electronics engineering from the Instituto Tecnológico de Celaya, Guanajuato, Mexico, in 2011, working in the area of digital signal processing, where she is currently pursuing the Ph.D. degree in engineering sciences in the area of electronic technologies. Her research interests include biotechnology, digital image processing, and instrumentation and control applications.

JUAN MARTÍNEZ-NOLASCO received the B.S. degree in electronics engineering from the Technological Institute of Guzman City, Jalisco, Mexico, in 2007, and the M.S. degree in electronics engineering and the Ph.D. degree in engineering science from the Technological Institute of Celaya, Guanajuato, Mexico, in 2009 and 2018, respectively. He is currently a Teacher and a Researcher with the Department of Mechatronics Engineering, Technological Institute of Celaya. His research interests include intelligent control, direct current microgrids, and applications of fuzzy logic control.